Applied Ocean Research **14** (1992) 175–190

Offshore pipe laying operations — Interaction of vessel motions and pipeline dynamic stresses

G.F. Clauss, H. Weede & T. Riekert

Institut für Schiffs-und Meerestechnik, Technische Universität Berlin, Salzufer 17-19, D-1000 Berlin 10, Germany

(Received 25 June 1991; accepted 2 April 1992)

Whereas numerous methods for the static analysis of pipelines during laying have been published, the dynamic analysis is still neglected. The numerical procedure presented in this paper allows for a systematic investigation of the significance of dynamic contributions in relation to static stresses and axial forces, with special emphasis on deep water laying procedures. Caused by waves and vessel motions during laying operations, the suspended pipespan will be subjected to dynamic bending and tension stresses as well as to substantial deflections. Based on large deflection beam theory, the paper presents a comprehensive dynamic analysis of pipelines under laying conditions. Numerical investigations illustrate the interaction of bending oscillations and dynamic tension. The results have been verified by model tests. The paper discusses the influence of vessel motion, water depth and pipe parameters on dynamic pipe stresses, motions and axial forces. Systematic investigations reveal the significance of pipeline dynamics depending on non-dimensional pipe characteristics. Superimposed to static stresses, the total stress distribution along the pipeline is evaluated. Depending on selected wave spectra and laying projects, the workability of specific laying vessels is illustrated and the influence of pipe dynamics analyzed.

NOTATION

$\tilde{b}(s)$	Linearized damping parameter
$b(s,t)$	Damping parameter
c_a	Morison's added mass coefficient = 1
c_d	Morison's drag coefficient
c_{ii}	Square of the first derivative of the ith normalized mode shape, integrated over the length
d	Vertical distance from seabed to top of stinger circle (S-lay method) or to the clamped end (J-lay method)
D	External diameter of steel pipe
D_c	Largest diameter, diameter of concrete coating
e_x, e_y, e_z	Cartesian vector base in the static touch-down point on the seabed: x = ahead, y = port, z = up
E	Modulus of elasticity of the steel pipe
EA	Axial rigidity of steel pipe
EI	Flexural rigidity of steel pipe
$F_s(s,t)$	Effective tension force = real tension force + displacing cross-sectional area times external hydrostatic pressure
$F_{sdy}(t)$	Dynamic part of effective or real tension force
F_{sj}	jth complex Fourier coefficient of the linearized dynamic tension force
$F_{sst}(s)$	Static part of effective tension force
g	Gravity acceleration = $9{\cdot}81\,m/s^2$
H	Horizontal tension force (effective static horizontal internal force)
k	On the soil: beam subgrade modulus; in the free span: $k = 0$
L	Unsupported length
m	Total mass per length of pipe including added mass in water or on soil, respectively
m_0	Mass per length of the pipe
$M_T(s,t)$	Torque
$M_{Tj}(s)$	jth complex Fourier coefficient of torque
n	Pipe ovalization, i.e. the maximum out-of-roundness $n = \Delta D/D$ (see Section 3)
$p_B(s,t)$	Like p_N, but perpendicular to the static plane
$p_{Bi}(s)$	Like p_{Ni}, but perpendicular to the static plane
p_c	External hydrostatic pressure
p_{cr}	Collapse pressure of an exactly circular pipe without axial stresses
$p_N(s,t)$	Hydrodynamic lateral line load component from waves and current in the static plane
$p_{Ni}(s)$	In linear dynamics: ith complex Fourier

Applied Ocean Research 0141-1187/92/S05.00

	coefficient of the line load p_N in the static plane; in non-linear dynamics: ith coefficient of modal decomposition of p_N and mass and damping loads from the quasi-stationary part, eqn (33).
p_{perm}	Permissible external hydrostatic pressure
$r(s,t)$	Radius vector of pipe axis from static touch-down point
R	Stinger radius
s	Curve length from static touch-down point, upwards positive
t	Time
t_s	Steel wall thickness
$u_B(s,t)$	Dynamic bending deflections perpendicular to the static plane
$u_{Bj}(s)$	Like u_{Nj}, but perpendicular to the static plane
$u_i(s)$	ith mode shape
$u_N(s,t)$	Dynamic bending deflections in the static plane
$u_{Nj}(s)$	jth complex Fourier coefficient of the linearized bending deflections in the static plane
$u_{Nj}^{(0)}(s)$	Contribution to u_{Nj} from lateral loads and boundary conditions
$u_{Nj}^{(1)}(s)$	The contribution of the dynamic tension force to u_{Nj} is $F_{sj}u_{Nj}^{(1)}$
$u_s(s,t)$	Axial dynamic deflection
$u_{sL}(t)$	Boundary value of u_s at upper end of unsupported span
$u_{sV}(t)$	Vessel motion component axial to the upper end of the free span
$u_{0B}(s,t)$	Like u_{0N}, but perpendicular to the static plane
$u_{0N}(s,t)$	Quasi-stationary part of the dynamic bending deflections in the static plane
V	Static bottom support force
$v_B(s,t)$	External flow velocity lateral to the pipe perpendicular to the static plane
$v_N(s,t)$	External flow velocity lateral to the pipe in the static plane
w	Submerged weight per length (weight in air minus buoyancy)
$x_{st}(s)$	Horiz. component of planar static elastic line
$z_{st}(s)$	Vertical component of planar static elastic line
$\beta_{ij}(t)$	Damping parameter multiplied by the ith and jth mode shape, integrated over the length
$\Delta u_s(t)$	Axial pipe motion relative to the vessel
$\Delta u_{s0}(t)$	Known split-off term of Δu_s, eqn (34)
κ	$= \lvert r''(s)\rvert =$ curvature
κ_{Bi}	Reference to modally decomposed curvature, eqn (32)
κ_{Ni}	Reference to modally decomposed curvature, eqn (32)
μ_{ii}	Mass distribution m times square of ith mode shape, integrated over the length
ν	Poisson's ratio of the steel pipe
ξ	External pipe diameter/wall thickness
ρ	Specific mass of sea water = 1025 kg/m^3
σ_l	Axial stress
σ_y	Yielding stress
$\tau_{Bj}(t)$	Like τ_{Nj}, but perpendicular to the static plane
$\tau_{Nj}(t)$	Reference to modal decomposition of the bending deflections in the static plane, eqn (27)
$\varphi(s)$	Static inclination angle
$\lvert\varphi'(s)\rvert$	Static curvature $\kappa_{st} = \lvert\varphi'\rvert = \lvert r''_{st}\rvert$
ω_j	jth discrete circular frequency, i.e. $j \cdot \Delta\omega$
Ω_j	jth natural circular frequency
$()'$	$\partial/\partial s$
$\dot{()}$	$\partial/\partial t$
$()_L$	Boundary value at top of free span

1 INTRODUCTION

A very economic method of transporting oil and gas from offshore deposits is through underwater pipelines. There are more than 60 000 miles of offshore pipelines beneath the world's oceans, and approximately 3000 miles of new pipelines are constructed each year. They vary from 3-in (76·2 mm) flow lines with typical lengths of a few miles, transporting oil and gas from individual wellheads, to 56-in (1·42 m) pipelines, used to unload oil tankers at offshore terminals. A net of large diameter trunk lines with lengths of up to 300 miles between pump stations has been installed in the North Sea.[1] Pipelines are crossing the Norwegian trench (300 m deep) and the Strait of Sicily (610 m deep). At a water depth of 732 m the flow lines between wellheads and the template at the Green Canyon Block 29 project illustrate the capability of deep water pipeline installation and operation.

The significance of offshore pipelining is also reflected in the high costs. For example, at the Marlim Field (Brazil) the pipelines, flexible lines and risers account for 49% of the expenditure for the early production pilot project. Of the overall exploitation costs of US$ 6 billion, the share of the subsea equipment, pipelines, flowlines and risers (without completion and wet christmas trees) is estimated to be 37%.[2] Consequently, the improvement of pipe laying techniques and pipe dimensioning is an important objective, inspiring an intensive development of deep water pipe laying techniques during the last two decades.

By far the majority of all offshore pipelines have been constructed by the conventional laybarge method, i.e. the S-lay method. Figure 1 shows this technique in comparison to the J-lay method. The S-lay method is routinely used up to water depths of 300 m. In greater water depths, however, problems are encountered, which have been focused in Shell's Deepwater Pipeline Feasibility Study in the late seventies. In a summarizing publication, Langner and Ayers[3] identify the main

obstacles to increasing the laying depth of offshore pipelines:

— Resetting of anchors takes more time than welding of the pipe. Further, the mooring characteristic becomes too soft, as the mooring lines are very long; dynamic positioning instead of mooring may become necessary.

— The stinger length has to be increased according to the steepness of the free span. Insufficient stinger length does not allow the pipe to leave this circular arc smoothly but results in a single-point support force at the last roller, introducing a huge bending moment peak. Such a long stinger experiences high loads itself, and either has to be stiff, or should provide sufficient buoyancy.

— The combined bending and circumferential stresses in the sag bend become more severe in deeper waters. Thus, the wall thickness of the pipe has to be increased to prevent a bending/buckling failure. This results in large pipe weight, associated with significant welding and laying problems.

— For suspending the long free span of the heavy pipe and limiting the curvature in the sag bend, tensioners with high capacity are required.

In spite of these problems, the Shell study came to the conclusion that laying 30-in (0·762 m) pipes with modern, so-called 'third-generation' lay barges (e.g. LB 200, CASTORO SEI, SEMAC 1) is practicable in water depths up to 600 m. Laying operations in greater depths seem feasible after modification of the lay barges, with the ultimate limitations being the stinger and the mooring system (unless the J-lay method and dynamic positioning are used). With reel barges, which unspool long sections of small diameter pipe (maximum 16 in (0·406 m)) from a big reel, laying of 12-in (0·305 m) pipe should be possible up to 2100 m water depth. Purpose-build J-lay vessels are expected to have even greater capabilities.[3]

A totally different solution for pipelaying problems represents the tow methods. In this case, long sections of pipe are manufactured ashore and pulled to their final location near the water surface or at the sea bottom. These two methods are promising, especially in deep water.[4]

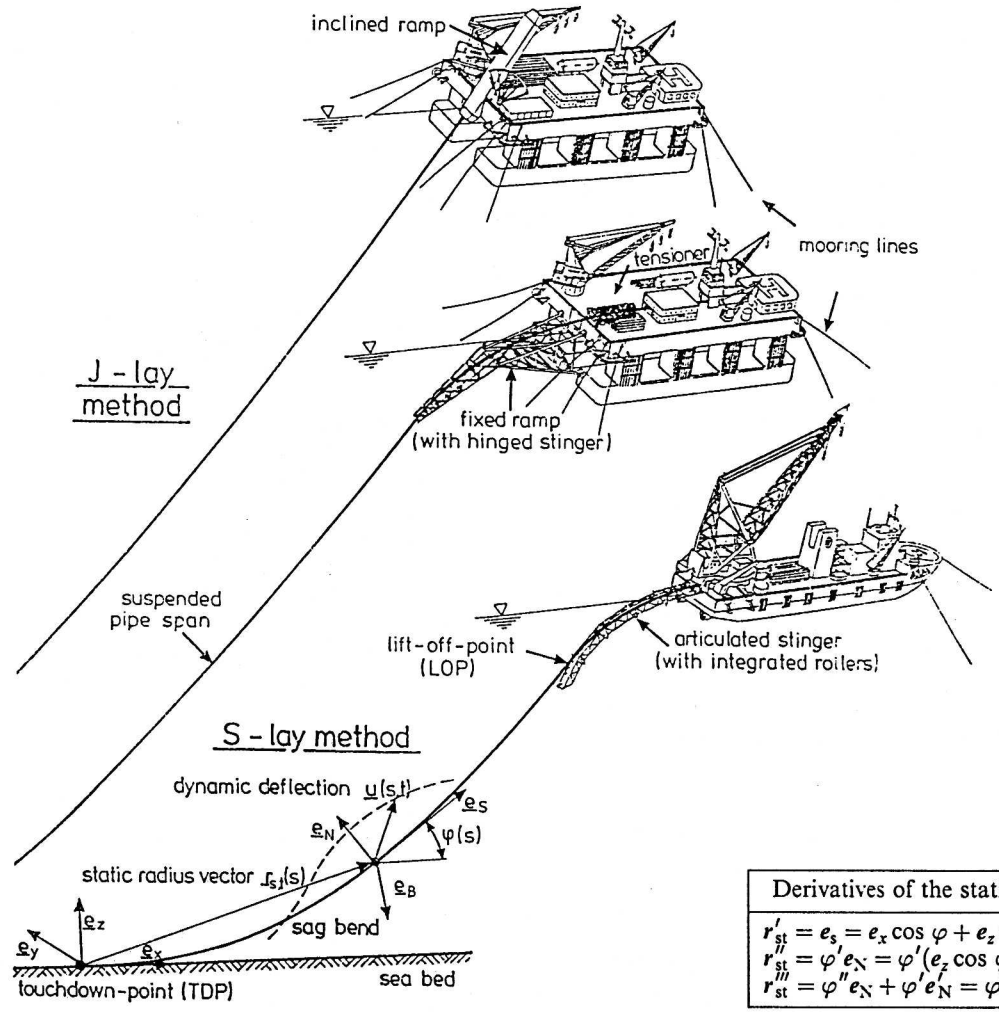

Derivatives of the static radius vector
$\underline{r}'_{st} = \underline{e}_s = \underline{e}_x \cos\varphi + \underline{e}_z \sin\varphi$
$\underline{r}''_{st} = \varphi' \underline{e}_N = \varphi'(\underline{e}_z \cos\varphi - \underline{e}_x \sin\varphi)$
$\underline{r}'''_{st} = \varphi'' \underline{e}_N + \varphi' \underline{e}'_N = \varphi'' \underline{e}_N - \varphi'^2 \underline{e}_s$

Fig. 1. Pipe laying in moderate and deep water by S-lay and J-lay methods.

After publication of the Shell study some pipelines have been laid in rather deep water (see paragraphs (1)–(5)).

(1) In connection with the Jolliet project in the Gulf of Mexico, two pipelines were laid down to 540 m water depth. For the deepest parts, flexible pipes were chosen with inner diameters of 8 in (0·203 m) and 10 in (0·254 m) respectively. One reason for selecting flexible pipes was their superiority at difficult seafloor conditions on the continental slope. They are connected to steel pipelines with outer diameters of 10 in (0·254 m) and 14 in (0·356 m), respectively, which were laid to a maximum depth of 430 m. During the laying with a second-generation barge, the progress in the deeper parts was hampered by problems with anchor handling and with repositioning of the vessel.[5]

(2) At the Green Canyon Block 29 development, close to Jolliet, pipelines were installed to connect the subsea template in 465 m water depth with a fixed production platform (14 in (0·356 m) and 16 in (0·406 m) diameter, respectively). The deep water sections of 10 miles length were installed by the bottom tow method, which was used for the first time in the Gulf of Mexico. Both lines were towed over the amazing distance of 430 miles.[6] Even into deeper waters, down to 732 m, flow lines have been laid from the template to remote subsea wellheads.

(3) At the Marlim Field (Brazil) a floating production system (FPS) with satellite wells is used for early production. The FPS, which is anchored in 600 m water depth, is connected to all wells and the two offloading buoys by flexible lines (maximum diameter 8 in (0·203 m)), running as deep as 750 m. A rigid 8 in (0·203 m) pipeline is used for gas export, but at the FPS this line is connected to a flexible line and riser, too. For the final development a 38 in (0·965 m) steel pipeline down to a depth of 700 m is proposed.[2]

(4) One of the longest and deepest pipe laying projects in hostile waters was the installation of the Statpipe System with a total length of 842 km which involved twice crossing of the 300 m deep Norwegian Trench. For this deepest tract a 30 in (0·762 m) X65 pipeline with a wall thickness of 22·2 mm was selected. Concrete coating thickness requirements were ranging from 45 to 115 mm, depending on location. The pipeline was laid with the 'third-generation' semisubmersible lay barge LB 200 (formerly Viking Piper) with a tensioner capacity upgraded from 1·33 to 2 MN and a refurbished fixed stern ramp.[7]

(5) Up to now, the deepest pipeline conventionally laid is the trans-Mediterranean Pipeline from Tunisia to Sicily. It consists of three 20 in (0·508 m) lines with 19·05 mm wall thickness for depths up to 280 m, increased to 20·62 mm for depths up to 610 m. The three lines were laid one after another between December 1979 and January 1981 with the third-generation laybarge CASTORO SEI, using the S-lay method with a laying ramp which has the capability of setting lift-off angles up to 40°. The installation had to be interrupted several times due to severe weather conditions. When the operation of the anchor handling tugs was affected, waiting on weather with the pipe being suspended resulted in substantial cyclic loading with potential fatigue damage.[8]

In conclusion, despite its long and intensive experience in laying offshore pipelines, the industry is still very cautious in advancing towards great water depths. In recent years, for many deep water projects flexible pipes were chosen, although conventional laying would also have been possible. Obviously, there still exist some uncertainties in the evaluation of the feasibility of pipe lay operations, especially in heavy seas.

Pipe dynamics during laying is the main objective of this paper, which discusses this phenomenon in close relation to the dimensioning of pipelines for deep waters. These two problems are mutually related, since the combined bending/buckling problem in the sag bend is crucial for dimensioning of the pipe wall thickness in deep water, and the dynamic bending in some cases contributes substantially to the total stress. The knowledge of the dynamic behavior is also important for the prevention of fatigue failure when the pipe laying process has to be interrupted due to severe weather conditions.

2 BENDING/BUCKLING DESIGN CRITERIA

As shown in Fig. 1, the pipeline is held on board by tensioners at the stern of the laying vessel. At its upper end, the pipe is supported by a stinger or a ramp. With the S-lay method, the required stinger length becomes minimum if the curvature κ of the pipe is constant, and follows from the maximum permissible longitudinal stress (due to bending and tension) according to $\kappa = 2\sigma_{\text{perm}}/(DE)$. D is the steel pipe diameter and E its modulus of elasticity.

In the sag bend, the maximum longitudinal stress, which the pipe material experiences farthest from the neutral bending plane, is superimposed to the circumferential stress due to the external hydrostatic pressure. Pipeline failure follows from the combined effects of bending, tension, and external pressure. In the following, the limiting pressure for avoiding a bending/buckling failure will be analyzed for pipes with an initial ovality or out-of-roundness due to imperfections during pipe manufacturing or handling, which is expressed in terms of the oval deformation ΔD related to the pipe diameter D, i.e. $n = \Delta D/D$.

Without longitudinal stress due to bending or tension, the critical collapse pressure of a circular pipe results from the action of uniform external pressure according to

$$p_{\text{cr}} = \frac{2E}{(1-\nu^2)\xi^3} \tag{1}$$

with the modulus of elasticity E, Poisson's ratio $\nu = 0{\cdot}3$, and the relation of pipe diameter and wall thickness $\xi = D/t_s$.[9] If in addition an initial ovality n of the pipe must be considered, the above relation is modified. Now the circumferential stress σ_φ due to an external pressure p_c follows from contributions of compressive force and bending moment:[9]

$$\sigma_\varphi = -\tfrac{1}{2}p_c\xi \pm \tfrac{3}{2}p_c\xi^2\frac{n}{1-p_c/p_{cr}} \tag{2}$$

The maximum of this circumferential stress σ_ϕ should not exceed the yielding stress σ_φ to avoid a buckling failure.

In the general case of a pipe with initial ovality, subjected to external pressure as well as to longitudinal stress σ_l due to bending and tension, the equivalent stress σ_e is calculated from the maximum contributions of circumferential stress σ_φ and longitudinal stress σ_l according to the distortion energy hypothesis:

$$\sigma_e = \sqrt{\sigma_l^2 + \sigma_\varphi^2 - \sigma_l\sigma_\varphi} \tag{3}$$

A pipe bending/buckling failure due to the combined effects of external pressure, bending and tension is avoided if this equivalent stress does not exceed the yielding stress σ_y. In the limiting case $\sigma_e = \sigma_y$, eqn (3) gives:

$$\sigma_\varphi = -\frac{\sigma_y}{2}\left[\sqrt{4-3\left(\frac{\sigma_l}{\sigma_y}\right)^2} - \frac{\sigma_l}{\sigma_y}\right] \tag{4}$$

Introducing eqns (2) and (1) into eqn (4), the permissible hydrostatic pressure p_{perm} for avoiding bending/buckling failures follows from:

$$p_{perm} = \alpha\frac{E}{(1-\nu^2)\xi^3}\left[1-\sqrt{1-4(1-\nu^2)\frac{\sigma_\varphi}{E}\left(\frac{\xi}{\alpha}\right)^2}\right] \tag{5}$$

with:

$$\alpha = 1 + 3n\xi + (1-\nu^2)\frac{\sigma_\varphi}{E}\xi^2 \tag{6}$$

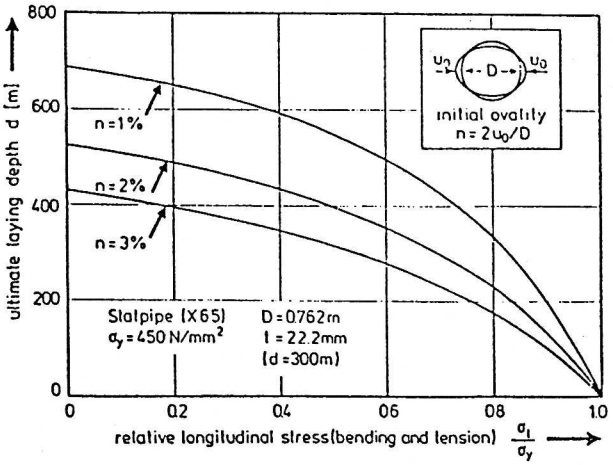

Fig. 2. Ultimate laying depth for yielding of steel pipe.

and σ_φ according to eqn (4).[10] Thus, the ultimate depth $d = p_{perm}/\gamma_w$ for laying pipelines of initial ovality n in waters of specific gravity γ_w depends on the ratio of pipe diameter and wall thickness, $\xi = D/t_s$, as well as on the relative longitudinal stress σ_l/σ_y. Note that the limiting parameter is the yielding stress, i.e. plastic deformations are excluded in the above analysis. With this condition, Fig. 2 gives the ultimate laying depth of a specified X65 pipeline at various initial ovalities. With higher relative longitudinal stress the ultimate laying depth is decreasing rapidly. Consequently, pipe laying with high tensioner capacity providing a low sag bend curvature is favorable.

At deep waters the limiting parameter is the stinger length. Thus, higher tension forces must be applied as would be required from bending/buckling criteria. Consequently, the resulting sag bend curvature and the associated longitudinal stress are less severe, permitting a higher initial ovality (see Fig. 2). Note that the ovality may be increased by plastic bending deformations at the stinger if its curvature is further enhanced. The analysis of plastic effects, however, is not within the scope of this paper, and the authors refer to Corona and Kyriakides,[11] who published a profound analysis of the response and the stability of pipes under combined bending and external pressure including plastic deformations. Their numerical results, verified by experiments, indicate that

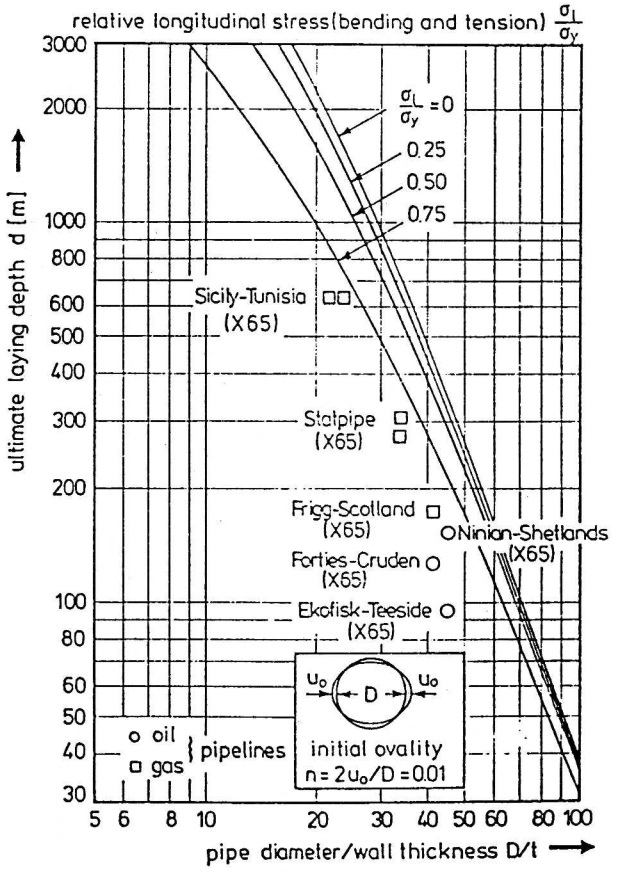

Fig. 3. Ultimate laying depth for yielding of steel pipe ($\sigma_y = 450\,N/mm^2$; $n = 1\%$).

the ultimate laying depth can be increased if plastic deformation is acceptable. The problem is very complex, as the critical combinations of pressure and curvature depend on the loading path. However, with low pipe curvature, ultimate water depths are quite similar, regardless whether elastic or plastic stress limitations are considered. Plastic deformation effects are especially important at high levels of curvature.

As mentioned before, this paper is based on the more conservative approach of limiting the equivalent stress by the yielding stress. Figure 3 shows the ultimate laying depth of X65 pipelines with an initial ovality of $n = 1\%$. In addition, the diagram presents design data of selected pipelines. From Fig. 3 it may be suggested that a relative longitudinal stress of $\sigma_l/\sigma_y = 0{\cdot}75$, due to static bending and tension, is acceptable. However, dynamic stress arising from laybarge motions in the seaway, or from operations like pipe pay-out and vessel move-up, have to be superimposed to static stresses. Thus, the following section will be devoted to the dynamic analysis of pipelines during laying.

4 STATIC AND DYNAMIC STRESSES OF PIPELINES DURING LAYING

This section presents the static and dynamic characteristics of pipelines during laying. The theoretical analysis of pipe motions and stresses induced by laying vessel motions is based on a profound theoretical investigation of oscillations of slender beams in a fluid excited by arbitrary line forces or motions at the beam's end.[12] The theory has been validated by model tests: the model testing technique achieves model similarity by defining characteristic numbers derived from the non-dimensional differential equation of pipeline dynamics.[13] Both the theoretical analysis and the model testing technique have been substantially improved.[14–16]

4.1 Basic equations

The pipe configuration is defined by the radius vector $r(s, t)$ of the pipe axis and the torsional angle $\chi(s, t)$ as functions of curve length s and time t, where $()' = \partial/\partial s$ and $(\dot{}) = \partial/\partial t$.

We regard a pipe element, length ds, loaded by an external line load q and internal forces F and moments M at both ends.

As the hydrostatic pressure is only acting on the wetted surface, the resulting force is normal to the pipe axis. It is easier, however, to substitute this force by:

— a vertical buoyancy force which summons the pressure on the wetted surface and the non-wetted cross-sectional areas; and, for appropriate correction,

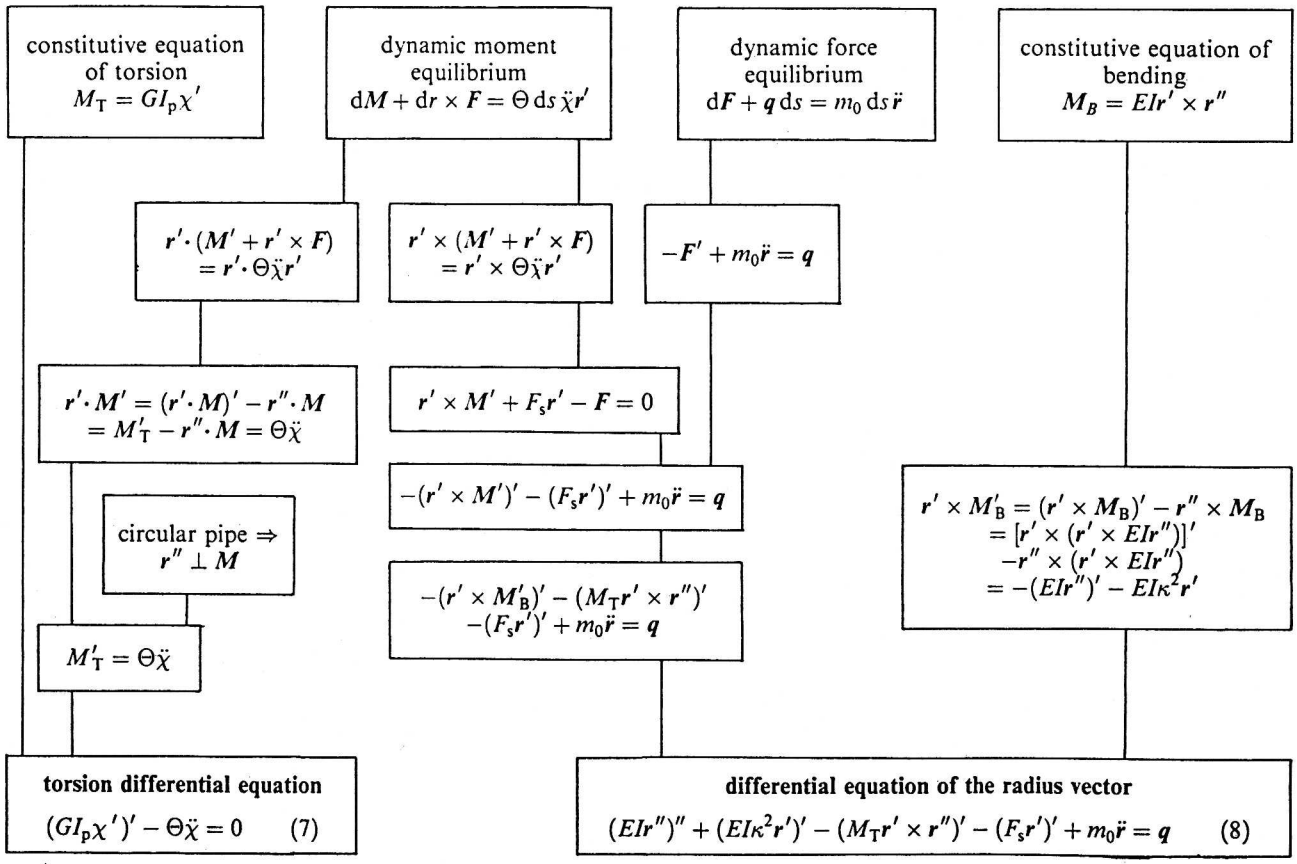

Table 1. Large deflection beam theory for circular pipes.

— axial tension forces which result from multiplying the external hydrostatic pressure by the cross-sectional areas.

The vertical buoyancy contributes to the external line load vector $\boldsymbol{q}$, and the axial tension forces are added to the internal force vector, i.e. the resultant 'effective' force $\boldsymbol{F}$ consists not only of the stress relevant forces, but also of these axial hydrostatic force contributions.

The basic equations are derived from the dynamic force and moment equilibrium and from the constitutive equations of bending and torsion of circular pipes. This derivation is illustrated similar to a flow-chart in Table 1 and results in the torsional differential eqn (7) and the differential equation of the radius vector eqn (8).

The radius vector $\boldsymbol{r}(s,t)$ of the pipeline is split into a planar static configuration $\boldsymbol{r}_{st}(s)$ and a dynamic deflection $\boldsymbol{u}(s,t)$ (see Fig. 1). To derive the planar static problem, we delete the inertia and torsional terms in eqn (8) and introduce the load $\boldsymbol{q} = -we_z$, i.e. the submerged weight per pipe length.

Next, eqn (8) is integrated, and the static radius vector is substituted by the static inclination angle $\varphi(s)$ (see Fig. 1). The lateral component of this equation,

$$EI\phi''(s) - H\sin\phi(s) + (ws - V)\cos\phi(s) = 0 \qquad (9)$$

where H is the horizontal tension force and V is the bottom support force, serves for determining the static configuration. A numerical solution and an analytical approach has been published by Weede.[12] The inclination angle $\varphi(s)$ yields the static curvature $|\varphi'(s)|$ for the static bending stresses and the static effective tension force $F_{sst}(s) = H\cos\varphi + (ws - V)\sin\varphi$.

The dynamic configuration is also calculated from eqn (8) (Table 1) after splitting off the static terms. The remaining vector equation is decoupled and results in the lateral dynamic component equations:

$$EIu_N'''' - (F_s u_N')' + m_0\ddot{u}_N = \varphi' F_{sdy} + q_{Ndy} \qquad (10)$$

$$EIu_B'''' - (F_s u_B')' + m_0\ddot{u}_B = (\varphi' M_T)' + q_{Bdy} \qquad (11)$$

where $u_N(s,t)$ is the dynamic bending deflection in the static plane and $u_B(s,t)$ that perpendicular to it.

On the left-hand side of eqns (10) and (11), the dynamic tension force F_{sdy} contributes to the effective tension force $F_s = F_{sst} + F_{sdy}$ introducing a time dependent stiffness. On the right-hand side, the dynamic tension force is combined with the static curvature $|\phi'(s)|$, resulting in a pseudo line load. By the constitutive equation of tension $F_{sdy} = EA\epsilon_{dy}$ the dynamic tension force is related to the dynamic strain:

$$\epsilon_{dy} = u_s' - \varphi' u_N + \frac{u_N'^2}{2} + \frac{u_B'^2}{2} \qquad (12)$$

which is a function of axial motions u_s and lateral motions u_N, u_B. Axial elastic vibrations are neglected, as the first axial natural frequency is too high to be excited by the seaway. Consequently, the dynamic tension force has nearly the same amplitude and phase all along the pipe, and may be averaged over the analyzed span.[12,17] This allows a significant simplification of the tensile problem coupled with bending: from the axial motion $u_s(s,t)$ only the boundary value $u_{sL}(t) = u_s(s = L, t)$ is relevant.

The hydrodynamic load components in the unsupported span, q_{Ndy} and q_{Bdy}, are deduced from the generalized Morison equation. If u is the lateral deflection of the moving pipe, and v is the lateral component of the flow velocity of waves and current, the dynamic load in the planar case may be expressed as:

$$q_{dy} - m_0\ddot{u} = \underbrace{\underbrace{(1 + c_a)\rho\frac{\pi D_c^2}{4}\dot{v} + \underbrace{c_d\frac{\rho}{2}D_c\,|\dot{u} - v|\,v}_{b(s,t)}}_{p(s,t)} - \underbrace{\left(m_0 + c_a\rho\frac{\pi D_c^2}{4}\right)}_{m}\ddot{u} - \underbrace{c_d\frac{\rho}{2}D_c\,|\dot{u} - v|\,\dot{u}}_{b(s,t)}} \qquad (13)$$

where m is the effective mass per unit length, $b(s,t)$ is the damping parameter and $p(s,t)$ is the load contribution from waves and current.[18]

Beyond the touch-down point, the pipe on the sea floor is treated as a generalized Winkler beam with linear elasticity, damping and inertia forces. k is the beam subgrade modulus (i.e. the restoring force coefficient), b expresses soil damping, and m includes soil added mass.

Introducing a three-dimensional version of eqn (13) and linearized soil reactions into eqns (10) and (11), the equations of dynamic bending in the static plane (N) and perpendicular to it (B) are obtained in their final version:

$$EIu_N'''' - (F_s u_N')' + ku_N + m\ddot{u}_N + b\dot{u}_N = \varphi' F_{sdy} + p_N \qquad (14)$$

$$EIu_B'''' - (F_s u_B')' + ku_B + m\ddot{u}_B + b\dot{u}_B = (\varphi' M_T)' + p_B \qquad (15)$$

where the damping parameter b in the free span follows from eqn (13):

$$b(s,t) = c_d\frac{\rho}{2}D_c\sqrt{(\dot{u}_N - v_N)^2 + (\dot{u}_B - v_B)^2} \qquad (16)$$

For deriving the relation between the dynamic tension force F_{sdy} and the axial pipe motion at the upper end of

the free span, u_{sL}, the constitutive equation of tension ($F_{sdy} = EA\epsilon_{dy}$) is combined with eqn (12) and averaged over the analyzed span:

$$F_{sdy}(t) = \frac{EA}{L}\left[u_{sL} - \int_{(L)}\left(\varphi' u_N - \frac{u_N'^2}{2} - \frac{u_B'^2}{2}\right) ds\right] \quad (17)$$

which is equivalent to

$$u_{sL}(t) = \frac{L}{EA}F_{sdy} + \int_{(L)}\left(\varphi' u_N - \frac{u_N'^2}{2} - \frac{u_B'^2}{2}\right) ds$$

Equation (17) reflects the fact that the tensioner drive may be operated in two different modes: if the tensioner is blocked, there is no relative motion between pipe and tensioner. In this case the boundary axial motion $u_{sL}(t)$ equals the associated vessel motion component $u_{sV}(t)$, and the dynamic tension force $F_{sdy}(t)$ is initially unknown. Alternatively, the tensioner drive may pay out or haul the pipe to keep the tension force on a constant value (compensating tensioner). In this case F_{sdy} is zero, and eqn (17) yields the boundary axial deflection $u_{sL}(t)$ at the upper end of the pipeline. Combined with the associated vessel motion $u_{sV}(t)$, the relative axial motion Δu_s between vessel and pipe follows from:

$$\Delta u_s(t) = u_{sL}(t) - u_{sV}(t) \quad (18)$$

4.2 Linear dynamic solution

The dynamic deflections and the corresponding dynamic tension force are calculated from eqns (14), (15) and (17). Linearization consists of four assumptions:

- The total effective tension force $F_s(s,t)$ on the left-hand side of eqns (14) and (15) is approximated by its static value $F_{sst}(s)$.
- The square strain terms in eqn (17) are neglected.
- For the hydrodynamic damping parameter $b(s,t)$ a time independent approximation $\tilde{b}(s)$ is adopted and improved iteratively to minimize the square error of the drag force.
- The tensioner operation mode — blocked or compensating — is not changing.

With these assumptions, eqns (14), (15) and (17) as well as their dynamic boundary conditions, i.e. the vessel motions, are converted to frequency domain using the general definitions:

$$f(t) = \sum_{j=-n}^{n} f_j e^{i\omega_j t} \qquad f_j = \frac{1}{T}\int_{(T)} f(t) e^{-i\omega_j t}\, dt$$

where f_j are the complex Fourier coefficients and $\omega_j = j \cdot 2\pi/T$ are the circular frequencies, with T being a sufficiently large time window.

The Fourier transform of eqn (14) cannot be solved directly if the tensioner is blocked, as the complex Fourier coefficients F_{sj} of the dynamic tension force are unknown in this case.

Introducing

$$u_{Nj} = u_{Nj}^{(0)} + F_{sj} u_{Nj}^{(1)} \quad (19)$$

the Fourier transform of eqn (14) is split into two equations for $u_{Nj}^{(0)}$ and $u_{Nj}^{(1)}$ whose right-hand sides are known. $u_{Nj}^{(0)}$ is the contribution from vessel motions, waves and current and has to be calculated with inhomogeneous boundary conditions from the vessel motions; $u_{Nj}^{(1)}$ is the contribution from the dynamic tension force and has to be calculated with homogeneous boundary conditions (all boundary values being zero).

To obtain the relation between the complex Fourier coefficients of the dynamic tension force (F_{sj}) and those of the boundary axial motion (u_{sLj}), eqn (19) is introduced into the Fourier transform of eqn (17) neglecting the square terms:

$$F_{sj} = \frac{EA}{L}\left[u_{sLj} - \int_{(L)} \varphi'(u_{Nj}^{(0)} + F_{sj} u_{Nj}^{(1)})\, ds\right] \quad (20)$$

The resulting linearized dynamic problem has been reduced to three ordinary differential equations for the complex Fourier coefficients of the dynamic bending deflections or their components, respectively:

$$EIu_{Nj}^{(0)\prime\prime\prime\prime} - (F_{sst} u_{Nj}^{(0)\prime})' + (k - \omega_j^2 m + i\omega_j \tilde{b}) u_{Nj}^{(0)} = p_{Nj}$$

(boundary values from vessel motion) (21)

$$EIu_{Nj}^{(1)\prime\prime\prime\prime} - (F_{sst} u_{Nj}^{(1)\prime})' + (k - \omega_j^2 m + i\omega_j \tilde{b}) u_{Nj}^{(1)} = \varphi'$$

(boundary values = 0) (22)

$$EIu_{Bj}^{\prime\prime\prime\prime} - (F_{sst} u_{Bj}')' + (k - \omega_j^2 m + i\omega_j \tilde{b}) u_{Bj} = (\varphi' M_{Tj})' + p_{Bj}$$

(boundary values from vessel motion) (23)

An FEM-type solution of such differential equations is described in Weede.[12]

If the tensioner is blocked, eqn (20) has to be resolved with respect to the complex Fourier coefficients F_{sj} of the unknown dynamic tension force, and the solutions of eqns (21) and (22) have to be introduced into:

$$F_{sj} = \frac{u_{sLj} - \int_{(L)} \varphi' u_{Nj}^{(0)}\, ds}{\frac{L}{EA} + \int_{(L)} \varphi' u_{Nj}^{(1)}\, ds} \quad (24)$$

The complex Fourier coefficients of the bending deflections in the static plane can then be composed according to eqn (19).

In the alternative case, if the tensioner drive prevents any

Table 2. Non-linear dynamic analysis

mode shapes u_j and natural circular frequencies Ω_j from eqn (26)
μ_{ii} and c_{ii} from eqn (31)
obtain solutions u of $EIu'''' - (F_{sst}u')' + ku = 0$ with unity boundary values to compose u_{0N}, u_{0B} with oscillating boundary values
obtain the corresponding components of κ_{Ni}, κ_{Bi}, p_{Ni}, p_{Bi}, Δu_{s0} to be combined with the oscillating boundary values
initialize results of previous timestep as zero
loop over the time: $t = 0, \Delta t, 2\Delta t, 3\Delta t, \ldots$
read vessel motions (boundary values) from file
stabilization: during initial interval multiply boundary values by a weighting factor smoothly increasing from 0 to 1
update Morison's drag coefficient c_d; update b with linearly extrapolated velocity; obtain β_{ij} from eqn (31)
combine boundary values with prefabricated components for κ_{Ni}, κ_{Bi}, p_{Ni}, p_{Bi}, Δu_{s0} from eqns (32)–(34)
set search interval F_{min}, F_{max} to the given permissible range
$F_{sdy} = (F_{max} + F_{min})/2$
set the sum terms in eqns (28) and (29) to zero
introduce Newmark method into eqns (28) and (29) and resolve that with respect to τ_{Ni}, τ_{Bi}
until the sum terms in eqns (28) and (29) are good
relative axial deflection Δu_s from eqn (30)
$\Delta u_s > 0$? yes: $F_{max} = F_{sdy}$ / no: $F_{min} = F_{sdy}$
until precision of dynamic tension force F_{sdy} is reached
evaluate eqn (27) combining the prefabricated components of u_{0N}, u_{0B} with the boundary values
after numerical stabilization: write results to output file
obtain velocities and accelerations of τ-values (Newmark method) and assign results to previous timestep

dynamic tension oscillations, i.e. $F_{sdy} = 0$, eqns (19) and (20) are evaluated with $F_{sj} = 0$. In this case, u_{Nj} only consists of $u_{Nj}^{(0)}$ which follows from eqn (21). The complex Fourier coefficients u_{sLj} of the boundary axial motion follow from eqn (20) with $F_{sj} = 0$ and are used to determine the relative axial motion between pipe and vessel.

The numerical solution is embedded in two nested loops. The internal loop steps along the circular frequencies $\omega_j = j \cdot 2\pi/T$, $j = 0, 1, 2, \ldots$. As the first frequency is zero, all three-dimensional effects, neglected in the planar static solution, can be recovered here, especially loads from a steady current. The external loop

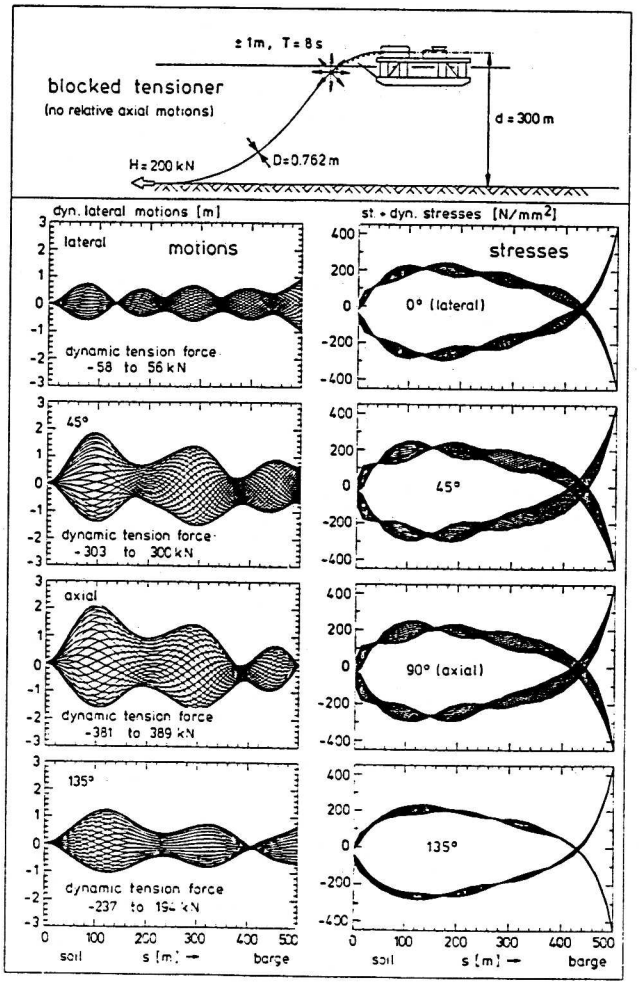

Fig. 4. Dynamics of offshore pipelines during laying — variation of excitation direction

serves to improve the linearized damping parameter:

$$\tilde{b}(s) = c_d \frac{\rho}{2} D_c \frac{\int_{(T)} [(\dot{u}_N - v_N)^2 + (\dot{u}_B - v_B)^2]^{3/2} \, dt}{\int_{(T)} [(\dot{u}_N - v_N)^2 + (\dot{u}_B - v_B)^2] \, dt} \tag{25}$$

The application of this formula may be speeded up by an approach presented by Krolikowski and Gay[19] for irregular seaway as a Gaussian process (see also Borgman[20]).

The mode shapes $u_j(s)$ and natural circular frequencies Ω_j, as needed in the next chapter, are calculated from:

$$EIu_j'''' - (F_{sst}u_j')' + (k - \Omega_j^2 m)u_j = 0 \tag{26}$$

which is the special version of eqns (21) and (23) for the undamped homogeneous case.

4.3 Nonlinear dynamic solution

The bending deflections $u_N(s,t)$, $u_B(s,t)$ are decomposed into modes shapes $u_j(s)$ and a quasi-stationary solution $u_{0N}(s,t)$, $u_{0B}(s,t)$ which satisfies the inhomogeneous

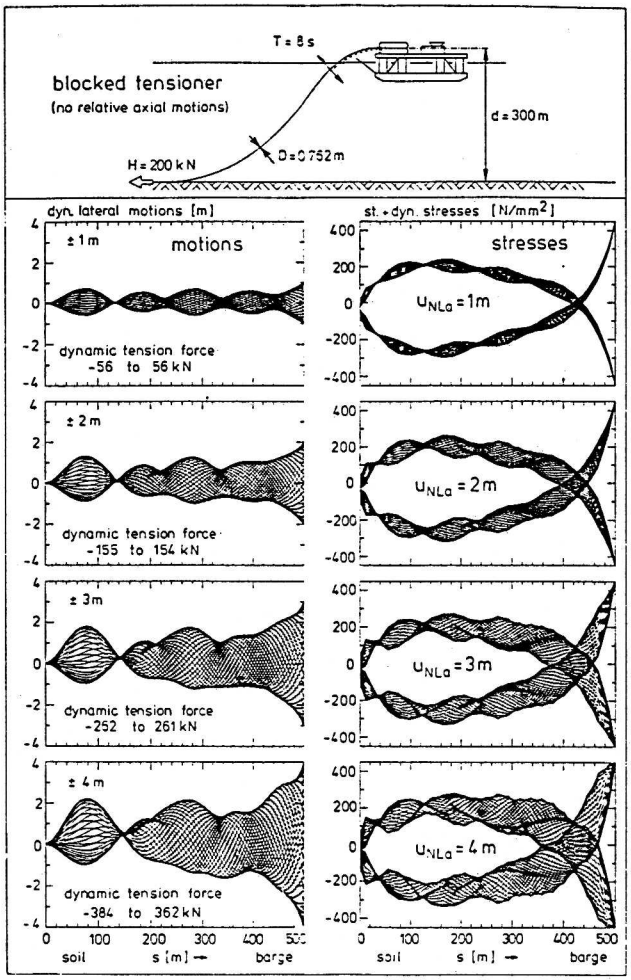

Fig. 5. Dynamics of offshore pipelines during laying — variation of lateral excitation amplitude

boundary conditions from the vessel motions:

$$u_N(s,t) = u_{0N}(s,t) + \sum_{(j)} u_j(s)\tau_{Nj}(t)$$
$$u_B(s,t) = u_{0B}(s,t) + \sum_{(j)} u_j(s)\tau_{Bj}(t) \tag{27}$$

The mode shapes $u_j(s)$ and the natural circular frequencies Ω_j follow from eqn (26). The quasi-stationary solution u_{0N}, u_{0B} may be superimposed from time independent components. Each of them is characterized by one individual boundary value being unity, and all others zero. They are calculated in advance before time simulation.

Equation (27) is introduced into the bending equations (14) and (15). These two partial differential equations are then multiplied by a mode shape and integrated over the analyzed span. This procedure converts them into two weakly coupled systems of ordinary differential equations:

$$\mu_{ii}\ddot{\tau}_{Ni} + \beta_{ii}\dot{\tau}_{Ni} + (\Omega_i^2\mu_{ii} + F_{sdy}c_{ii})\tau_{Ni} = F_{sdy}\kappa_{Ni} + p_{Ni} - \sum_{(j\neq i)} \beta_{ij}\dot{\tau}_{Nj} \tag{28}$$

$$\mu_{ii}\ddot{\tau}_{Bi} + \beta_{ii}\dot{\tau}_{Bi} + (\Omega_i^2\mu_{ii} + F_{sdy}c_{ii})\tau_{Bi} = F_{sdy}\kappa_{Bi} + p_{Bi} - \sum_{(j\neq i)} \beta_{ij}\dot{\tau}_{Bj} \tag{29}$$

Equation (27) is also introduced into eqn (17). This yields the relative axial motion between pipe and vessel as follows:

$$\Delta u_s = \Delta u_{s0} + \frac{L}{EA}F_{sdy} + \sum_{(i)}[\kappa_{Ni}\tau_{Ni} + \kappa_{Bi}\tau_{Bi} - \frac{c_{ii}}{2}(\tau_{Ni}^2 + \tau_{Bi}^2)] \tag{30}$$

The coefficients of this modal formulation of the problem are defined as:

$$\mu_{ii} = \int_{(L)} mu_i^2\,ds \quad \beta_{ij} = \int_{(L)} bu_iu_j\,ds\; c_{ii} = \int_{(L)} u_i'^2\,ds \tag{31}$$

$$\kappa_{Ni} = \int_{(L)} u_i\phi'\,ds - \int_{(L)} u_i'u_{0N}'\,ds$$
$$\kappa_{Bi} = -\int_{(L)} u_i'u_{0B}'\,ds \tag{32}$$

$$p_{Ni} = \int_{(L)} u_i[p_N - b\dot{u}_{0N} - m\ddot{u}_{0N}]\,ds$$
$$p_{Bi} = \int_{(L)} u_i[p_B + (\phi' M_T)' - b\dot{u}_{0B} - m\ddot{u}_{0B}]\,ds \tag{33}$$

$$\Delta u_{s0} = \int_{(L)} \left(\phi' u_{0N} - \frac{u_{0N}'^2}{2} - \frac{u_{0B}'^2}{2}\right) ds - u_{sV} \tag{34}$$

The time dependent damping parameter b is contained in β_{ii}, p_{Ni}, p_{Bi} and follows from the generalized Morison equation (13). It is updated at each time step by linear extrapolation of the bending velocity.

Both equation systems (28) and (29) are solved with the Newmark method.[21] The resulting $\tau_{Ni}(t)$, $\tau_{Bi}(t)$ are functions of the unknown dynamic tension force F_{sdy}. It is necessary to keep this tension within a design range. Consequently, F_{sdy} is controlled at each time step using the following procedure.

Equation (30) represents the relative axial motion as a function of the dynamic tension force. A binary search for the zero-crossing of this function aims to find the F_{sdy} which causes the tensioner to stop ($\Delta u_s = 0$). As the predefined permissible range is taken as initial search interval, F_{sdy} converges towards:

- a value which yields $\Delta u_s = 0$ if acceptable;
- the lower or upper limit if the required F_{sdy} would be too small or too large, respectively.

Thus, operation phases of blocked or compensating tensioner may alternate.

The algorithm is illustrated in Table 2. This dynamic analysis method has been validated with model tests.[15,16]

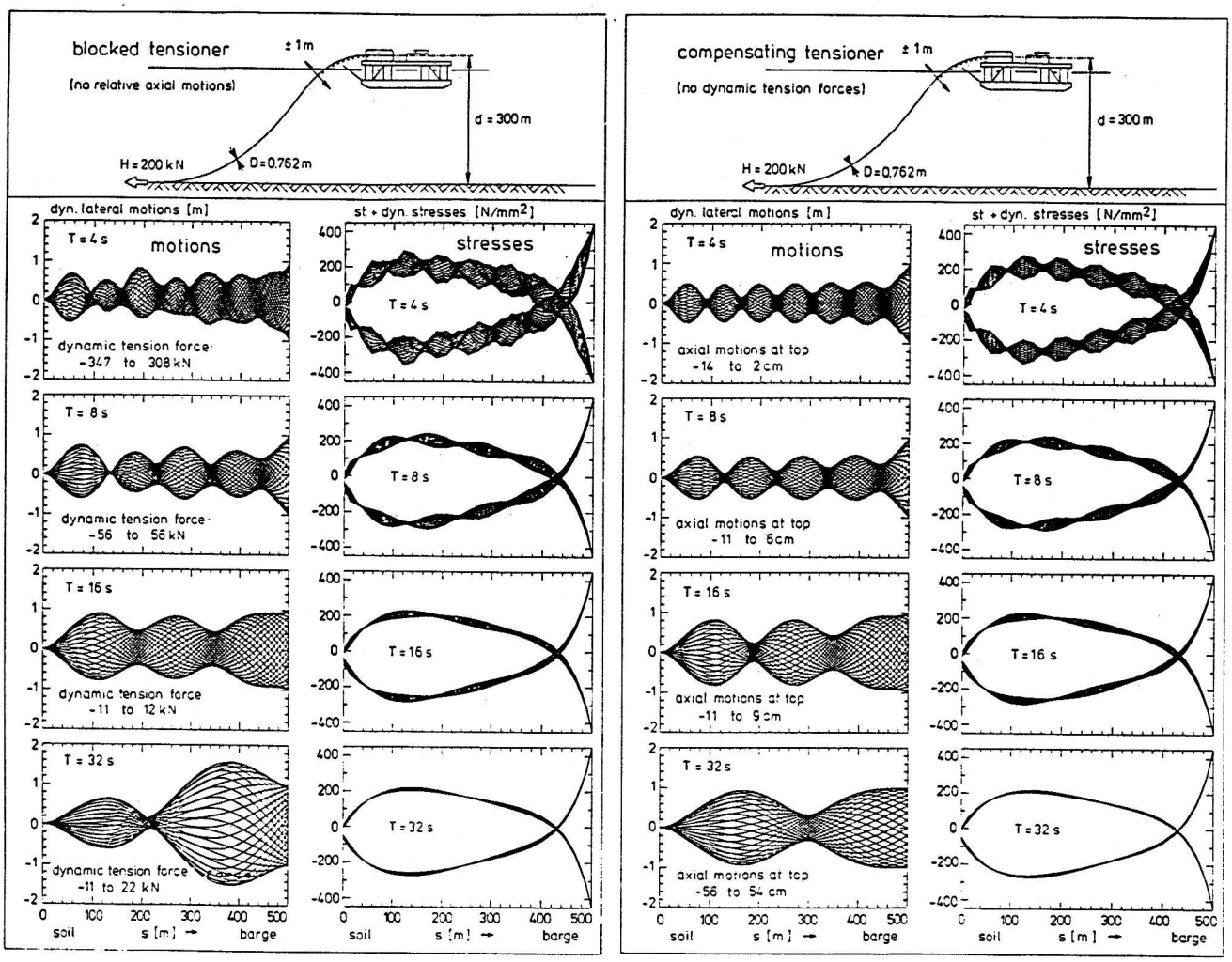

Fig. 6. Dynamics of offshore pipelines during laying — variation of motion (wave) period T (lateral excitation)

5 EXAMPLE CALCULATIONS

5.1 Influence of the system parameters

Finally, after validation of the theory, example calculations have been performed to illustrate the dynamic effects at typical laying operations. As a representative example, a 30-in pipeline ($D = 0{\cdot}762$ m) was selected. With a steel wall thickness of 22·2 mm, or $D/t_s = 34{\cdot}3$, a laying depth of $d = 300$ m is acceptable, if modern laying technique is used (see Fig. 3). Armoured by a 45 mm concrete coating, the submerged pipe weight per unit length is 784 N/m.

Figures 4–8 illustrate the dynamic lateral deflection and the corresponding stresses at different excitation modes. Note that the stresses are presented at the upper and lower fiber of the pipeline superimposing the static stress and the envelope of the dynamic effects. The diagrams show the influence of typical design parameters for both operation modes of the tensioner, blocked and compensating tensioner.

For a blocked tensioner, Fig. 4 illustrates the influence of excitation direction. Obviously, axial excitation results in severe lateral motions and dynamic stresses. Note the high level of dynamic tension force. Figure 5 gives the non-linear increase of motions and stresses with lateral motion amplitude, again for the operation mode of a blocked tensioner. Figures 6–8 demonstrate the influence of excitation period, tension force and laying depth on pipe dynamics. The left-hand diagrams illustrate the effects for blocked tensioner with subsequent high dynamic axial forces resulting in substantial non-linear effects, whereas the right-hand diagrams show the pipe behavior if the tensioner is compensating. In this case axial motions at the pipe's upper end are observed.

Comparing the two alternatives of blocked or compensating tensioner it is evident that any pipe laying procedure has to cope with high alternating axial tension forces or substantial relative motions between pipe and tensioner. Alternating axial tension forces are limited by the tensioner design capacity. The associated stress variations are illustrating the adverse effects of tensioner blockage, and it is evident that substantial motions of the vessel are prohibitive. In the second case, when the tensioner is pulling with a constant force, the pipeline experiences relative motions which are resulting from the pipe motions at top

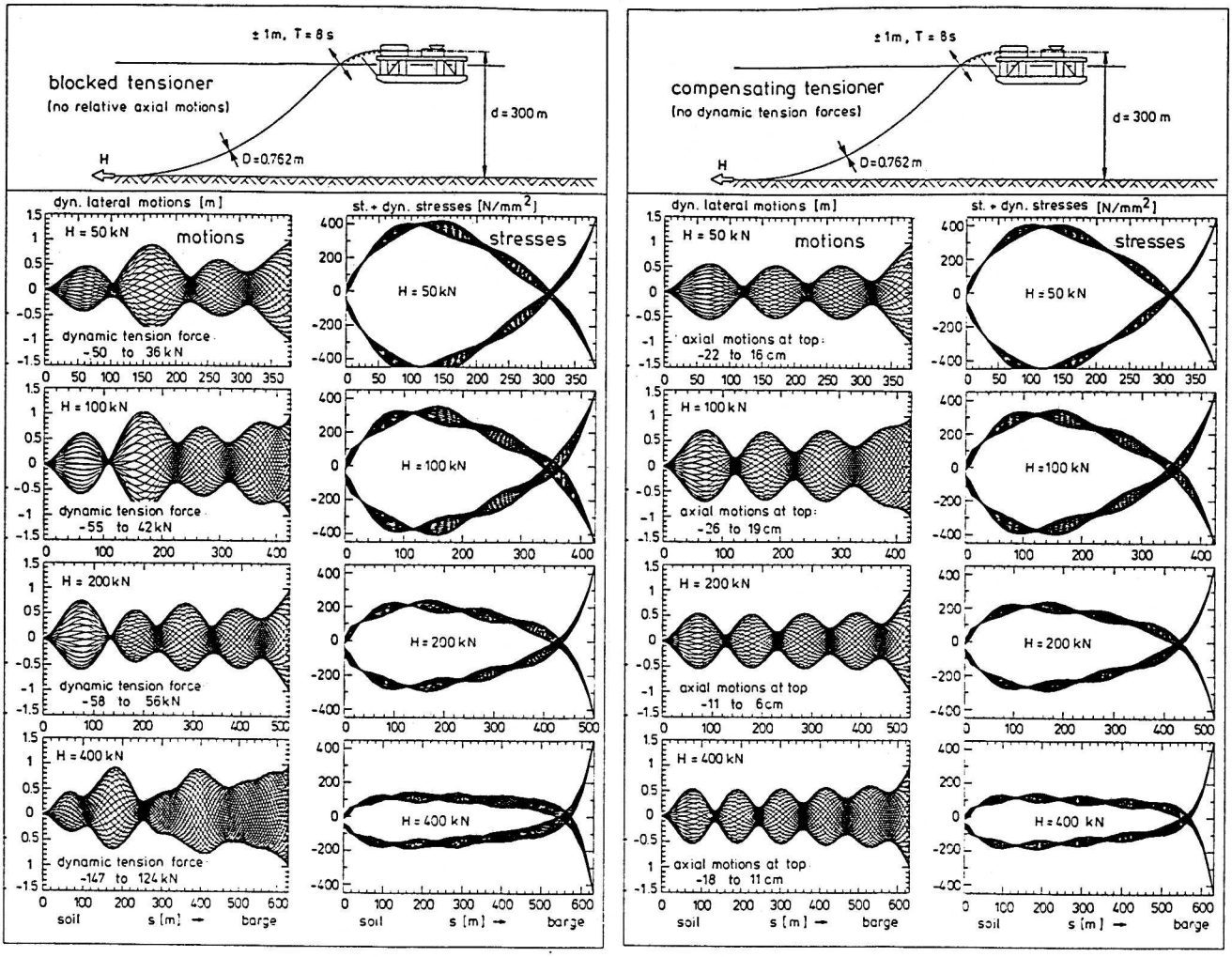

Fig. 7. Dynamics of offshore pipelines during laying — variation of horizontal tension force H (lateral excitation)

superimposed by the vessel motions with regard to the appropriate phase relation. In general, favorable motion characteristics are advantageous in all cases which explains the preference for semisubmersible laying vessels. For illustrating the significance of vessel motions on pipe dynamics in the seaway, the behavior of a typical laying vessel is analyzed.

5.2 Motion characteristics of the lay vessel LB 200

It is evident from the previous section that the knowledge of the motions of the lay vessel is a prerequisite for the analysis of pipeline dynamics in a natural sea state. As a typical lay vessel the semisubmersible LB 200 is chosen (Fig. 9). For the determination of the motions of the vessel the numerical program WAMIT is used, which has been developed at the Massachusetts Institute of Technology (MIT).[22] A discretization of the structure, represented by the corner points of the elements and the relations between points and elements, is used as an input file. Usually the coordinates are derived from a drawing and entered manually. This option is time consuming and prone to errors, especially if many elements are required. Further, it is difficult to change the elementation. Therefore, an improved method was developed which is based on the fact that offshore structures often consist of components with simple shapes, like circular cylinders, rectangular plates or pontoons. For the elementation of such fundamental shapes interactive FORTRAN subroutines were developed. For the discretization of a specific structure the subroutines are linked to a purpose-made main program in which the geometrical data of the structure like length, breadth, coordinates, and orientation of the individual components are defined. The number and distribution of the elements are determined by the program user. Once the program for a body exists, an elementation even with some hundred elements can be generated within a few minutes. For displaying the elementation on the screen graphic programs have been developed incorporating projections, programs for rotating the body, and algorithms for hidden line removal.

For the lay vessel LB 200, a discretization with 1024 elements was generated. Figure 9 presents this discretization as well as the magnitudes of the calculated

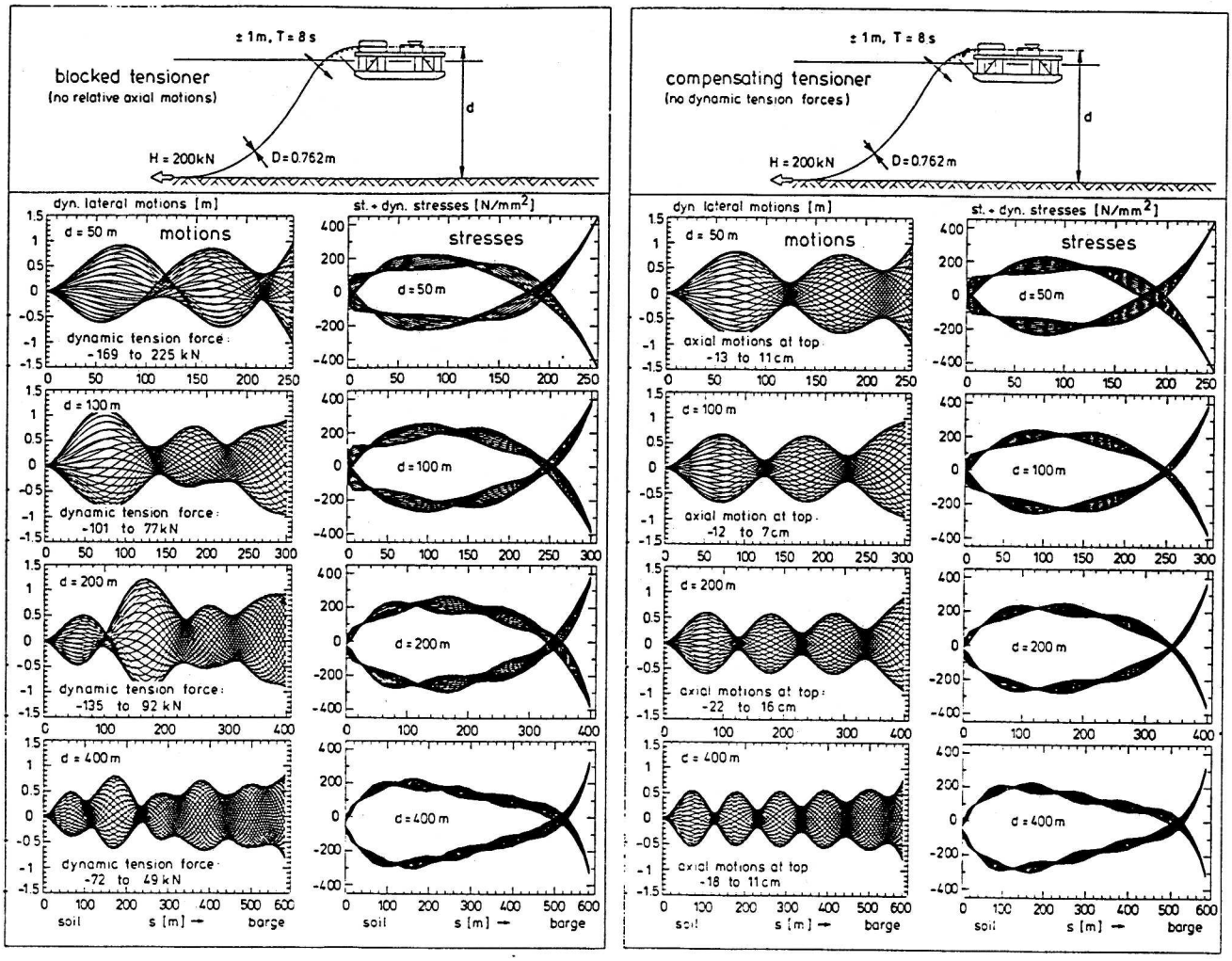

Fig. 8. Dynamics of offshore pipelines during laying — variation of water depth d (lateral excitation).

motion transfer functions of the LB 200 in head seas. A comparison between calculations and results of supervisory model tests (scale 1 : 100) proves the reliability of the method. By geometrical transformation of the (complex) transfer functions, related to the center of gravity, the motions of the lift-off point (LOP) at the stinger are determined. Note that they are related to the pipe coordinate system. Influenced by the vessel motions in all three degrees of freedom, these axial and lateral motions at the lift-off point show two resonance peaks which follow from heave and pitch of the vessel, respectively. As the calculations are carried out for finite water depth ($d = 300$ m), the surge motion increases to infinity with ω approaching zero.

Based on these transfer functions, the motions of the vessel in heavy seas are calculated. The energy spectra of waves and vessel motions are presented in Fig. 10.

For the description of the sea state, the JONSWAP-spectrum with significant wave height $H_s = 4{\cdot}5$ m, peak period $T_p = 7$ s, and shape factor $\gamma = 3{\cdot}3$ is selected. A comparison of the transfer functions in Fig. 9 and the motion behavior of the lay vessel in Fig. 10 reveals that the resonance peaks of heave and pitch are irrelevant for pipe excitation as the spectral energy in the low frequency band is insignificant. The selected wave spectrum represents a real storm which was experienced by the lay vessel on 22 March 1983. During this storm the LB 200 was not in pipe laying operation but anchored carefully.[23] A comparison of wave and motion calculations (see Fig. 10) with measurements on board the semisubmersible pipe laying barge demonstrate fair correspondence in the high frequency band which is decisive for the pipe excitation. At the low frequency band, however, the full scale measurements of the vessel motions show some severe inconsistencies which cannot be interpreted physically. This reveals that measurements on board of semisubmersibles are quite delicate, and misinterpretations could only be avoided if the results are backed up by theoretical investigations or model tests.

5.3 Pipe laying in irregular seas

In conclusion, the dynamic behavior of the entire pipe

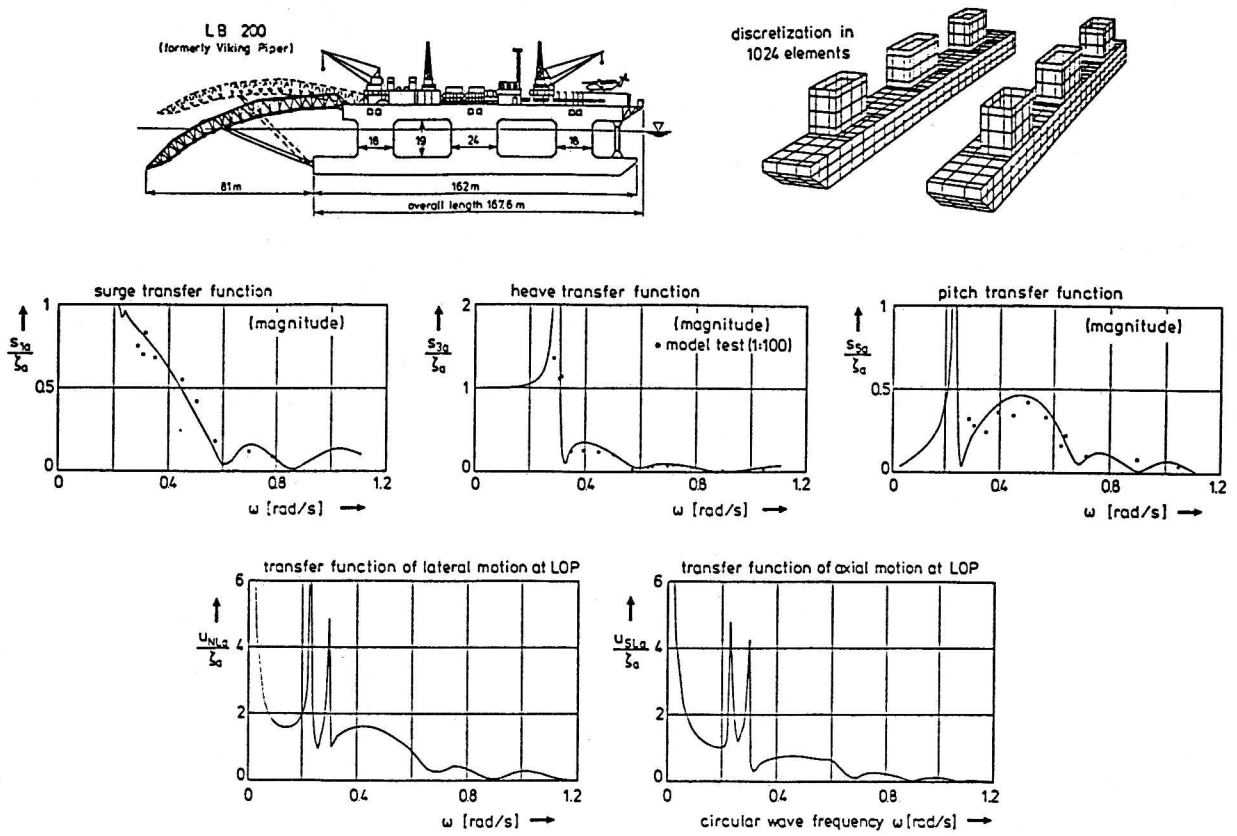

Fig. 9. Motion transfer function of laying vessel LB 200

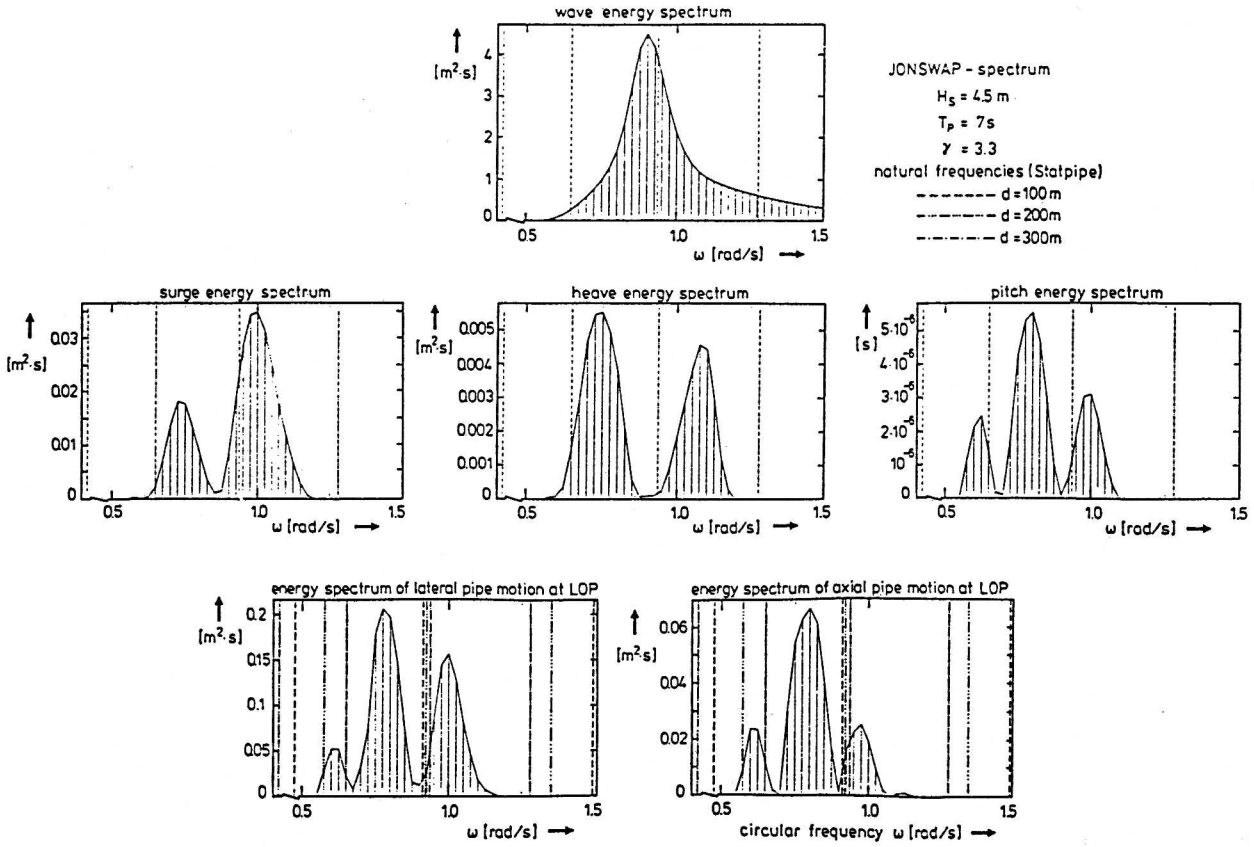

Fig. 10. Motion response of LB 200 in random waves

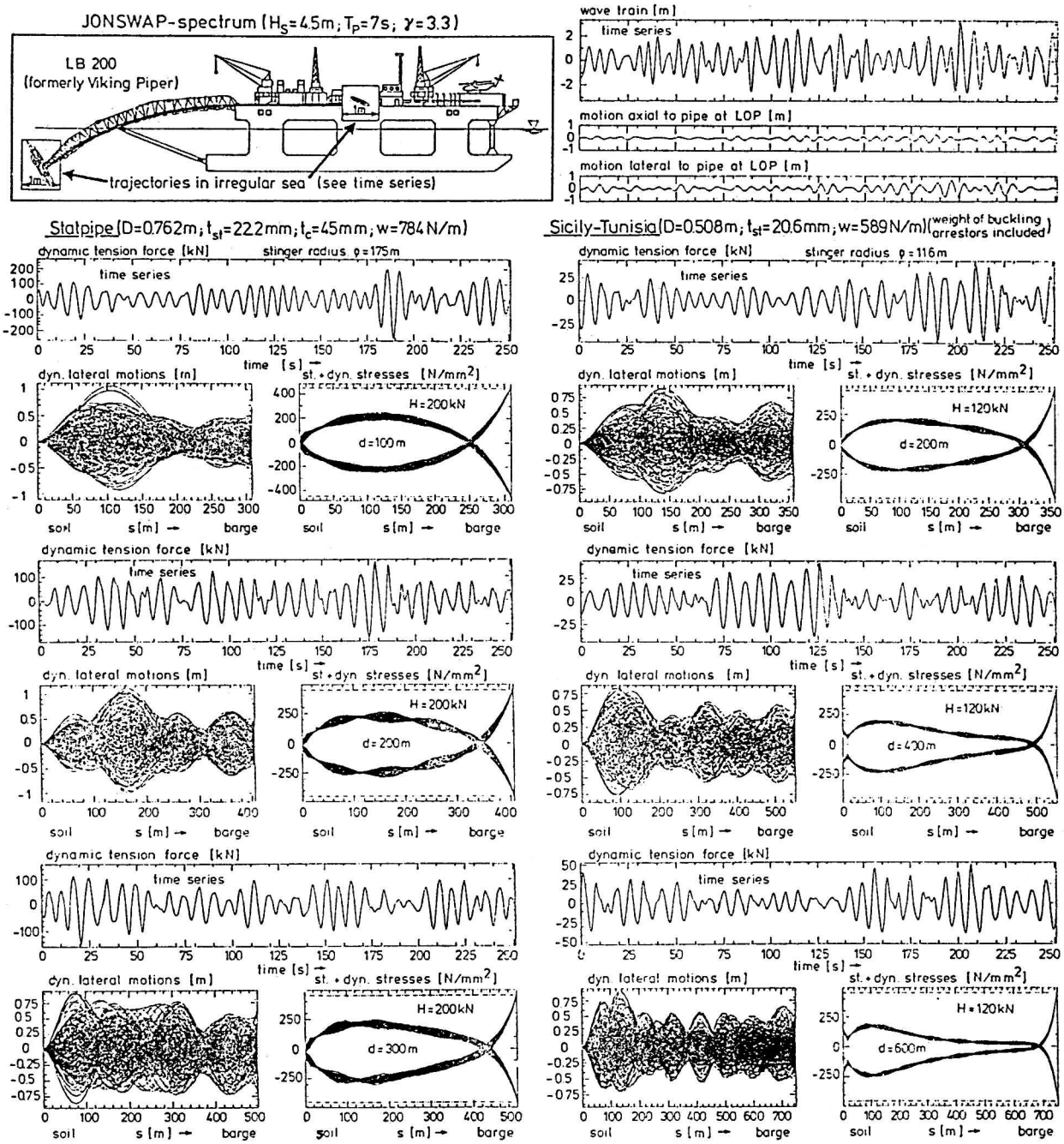

Fig. 11. Pipe laying in irregular seas ($H_s = 4{\cdot}5\,\text{m}$; $T_p = 7\,\text{s}$) — blocked tensioner

laying system is presented in Fig. 11 for the Statpipe and the Sicily–Tunisia pipeline. For each, the motions in a severe storm are simulated for three different laying depths. The pipe excitation follows from the vessel motions as presented in Figs 9 and 10. As shown in Fig. 11, the lift-off point at the stinger end experiences axial and lateral motions in the order of magnitude of about 1 m if the vessel encounters irregular seas with a significant wave height of $H_s = 4{\cdot}5\,\text{s}$ and a peak period of $T_p = 7\,\text{s}$. From the trajectories, shown in the upper part of the diagram, it follows that the transverse vessel motions at the center of gravity are small, so the LOP motions are dominated by pitch motions. Note that the stinger is supposed to be rigid. As the tensioner is operated in the blocked mode, large variations of the dynamic tension force are observed. Finally, the lower diagrams illustrate the dynamic lateral motions and the associated static and dynamic stresses along the pipe for various laying depths. These diagrams reveal that dynamic contributions are quite substantial and should be considered in the design process.

Note that the natural frequencies of the free pipespan for the Statpipe at different water depths are also marked in Fig. 10: each natural frequency is excited with different energy. Nevertheless, the dynamic response remains in the same order for all depths (Fig. 11). This

leads to the conclusion that the transfer function of the pipeline has nearly no resonance peaks due to hydrodynamic drag and soil damping. Consequently, the dynamic response will not increase remarkably if one natural frequency happens to coincide with a maximum of the excitation spectrum.

As a second example, the right-hand side of Fig. 11 illustrates the dynamics of the much deeper Sicily–Tunisia pipeline. If the same environmental conditions are considered, the motions of the lift-off point of the laying vessel are comparable. Note that the stinger radius is reduced to 116 m. The lateral pipe motions as well as the static and dynamic stresses are presented in the lower diagrams. As expected from results in Fig. 8, the dynamic stress contributions in greater laying depths are less significant. Further, it should be noted that the limiting parameter in deep water pipe laying is frequently the stinger length. As a consequence, higher tension forces must be applied as would be required from bending/buckling criteria. As a result, the bending stress in the sag bend may be so small, that a higher initial ovality can be accepted (see Fig. 2). In conclusion, a higher curvature in the overbend section on the stinger with subsequent plastic deformation may be permissible in certain cases.

In summary, it should be stated that pipe dynamics are a highly complicated problem, and sophisticated analytical tools are required to determine the significance of related motions and stresses.

6 CONCLUSION

The design of deep water pipelines is dominated by bending/buckling criteria in the sag bend region. Pipe bending depends on pipe weight and the lay vessel characteristics. Besides stinger length and its adaptability as well as tensioner and mooring capacity the motions of the lay vessel in the seaway are of major importance as they induce complicated bending oscillations and stresses of the pipe which must be considered in the design process. The paper exemplifies that environmental conditions, laying vessel characteristics, and pipe dimensions show complex interactions, and dynamic effects play an important role in the evaluation of the reliability of the laying process. Consequently, tailor-made investigations are required, using the numerical tools presented in this paper.

ACKNOWLEDGEMENTS

The authors are indebted to Mr H. Höhne for the careful preparation of all diagrams in this paper. They also wish to express their gratitude to Mr J. Heeg who assisted in the completion of the manuscript.

REFERENCES

1. Chung, J.S., Offshore pipelines. *Mechanical Engg*, May 1985, 64–9.
2. Massa, F.E.A., Challenging a deep sea giant. In Conf. on Deep Offshore Technology (DOT), Marbella, Oct. 1989.
3. Langner, C.G. & Ayers, R.R., The feasibility of laying pipelines in deep waters. In Offshore Mechanics and Arctic Eng. Symp. (OMAE), Dallas, Feb. 1985.
4. Brown, J.R., The next step: Installing pipelines in 5000 ft water. *Ocean Industry*, March (1990) 25–30.
5. Tillinghast, W.S. The deepwater pipeline system on the Jolliet project. In *OTC 6403*, 22nd Offshore Technology Conf., Houston, May 1990.
6. Cober, W.J., Filson, J.J. & Teers, M.L. An overview of the Green Canyon Block 29 development. In *OTC 5397*, 19th Offshore Technology Conf., Houston, April 1987.
7. Akten, H.T., Lund, S. & Miller, D.M. On the design and construction of Statpipe pipeline system. In *OTC 4922*, 17th Offshore Technology Conf., Houston, May 1985.
8. Bonfiglioli, G., The Trans-Med Pipeline. *Pipes & Pipelines Int.*, March/April (1986).
9. Timoshenko, S. *Theory of Elastic Stability*. McGraw-Hill, New York, 1936, pp. 204–38.
10. Clauss, G., Kruppa, C., Wolf, E. & Stamm, K., Parametric study for deep water pipelaying. *Meerestechnik mt*, **8** (No. 3, June) 1977.
11. Corona, E. & Kyriakides, S. On the collapse of inelastic tubes under combined bending and pressure. *Int. J. Solids Structures*, **24**(5) (1988).
12. Weede, H. Dynamik offshoretechnischer Linientragwerke am Beispiel der Pipelineverlegung. Dissertation, Technische Universität Berlin, 1990.
13. Clauss, G. & Kruppa, C., Model testing techniques in offshore pipelining. In *OTC 1937*, 6th Offshore Technology Conf., Houston, May 1974.
14. Clauss, G.F. & Weede, H., Dynamic stresses and motions of offshore pipelines during laying. In Offshore Mechanics and Arctic Eng. Symp. (OMAE), Stavanger, June 1991, Vol. V, pp. 17–24.
15. Clauss, G.F., Weede, H. & Saroukh, A., Offshore pipelaying — Significance of dynamic stresses and motions during laying operations. In *OTC 6760*, 23rd Offshore Technology Conf., Houston, May 1991.
16. Clauss, G.F., Weede, H. & Saroukh, A., Nonlinear static and dynamic analysis of marine pipelines during laying. *Schiffstechnik, Bd. 38 — 1991/Ship Technology Research*, **38** (1991).
17. Kauderer, H., *Nichtlineare Mechanik*. Springer Verlag, Berlin, 1958.
18. Clauss, G., Lehmann, E., Östergaard, C. *Meerestechnische Konstruktionen*. Springer Verlag, Berlin 1988.
19. Krolikowski, L.P. & Gay, T.A. An improved linearization technique for frequency domain riser analysis. In *OTC 5980*, 12th Offshore Technology Conf., Houston, May
20. Borgman, L.E., Ocean wave simulation for engineering design. *J. Waterways & Harbors Div., ASCE*, **95** (WW4) (1969) 557–83.
21. Burnett, D.S., *Finite Element Analysis*. Addison-Wesley, Reading, MA, 1987.
22. Newman, J.N. & Sclavounos, P.D., The computation of wave loads on large offshore structures. In Int. Conf. on Behaviour of Offshore Structures (BOSS), Trondheim, June 1988.
23. Wevers, L.J., Vlaming, M. & Verdonck, J., Wave and motion measurements on board the semisubmersible pipelaying barge LB 200. In *OTC 5028*, 17th Offshore Technology Conf., Houston, May 1985.